

COMPARING EXTENDED SYSTEM INTERACTIONS WITH MOTIONS IN SOFTENED POTENTIALS

ERIC I. BARNES

Department of Physics, University of Wisconsin — La Crosse, La Crosse, WI 54601
Draft version April 19, 2018

ABSTRACT

Using an N -body evolution code that does not rely on softened potentials, I have created a suite of unbound interacting cluster pair simulations. The motions of the centers of mass of the clusters have been tracked and compared to the trajectories of point masses interacting via one of four different softened potential prescriptions. I find that the relationship between the impact parameter of the cluster interaction and the point-mass softening length that best approximates each cluster’s center-of-mass motion depends on the adopted prescription. In general, the range of allowed softening lengths grows roughly linearly with the impact parameter, but zero softening is acceptable in the majority of situations. In an N -body simulation that adopts a fixed softening length, such relationships lead to the possibility of two-body effects, like dynamical friction, being either larger or smaller than the corresponding cluster situation. Further consideration of more specific N -body situations leads estimating that a very small fraction of point-mass encounters experience two-body effects significantly different than those of equivalent clusters.

Subject headings: methods:numerical — gravitation

1. INTRODUCTION

It is common for N -body integration schemes to rely on softened potentials to speed up calculations. Small impact parameter, two-body encounters in a Newtonian potential can drive timesteps to very small values in some N -body implementations (*e.g.*, Aarseth 2001, NBODY2). Softened potentials relax this behavior by capping the maximum acceleration any particle can experience, thereby placing a lower limit on the timestep. From another perspective, softened potentials allow an N -body system to behave more like a collisionless system, where two-body effects are absent. Minimizing strong scattering has led other N -body codes to adopt softened potentials (*e.g.*, Springel 2005, GADGET-2).

One way of bringing some physical reality to the idea of using softened potentials is to imagine that each particle in a simulation is actually a cluster of unresolved particles. This work investigates the interactions of binary clusters of particles relying strictly on Newtonian potentials (but note that throughout this work these clusters are not bound to one another). This is made possible by using the graphics processing unit (GPU) enhanced version of Aarseth’s NBODY6 code (Aarseth 2003; Nitadori & Aarseth 2012). For comparison purposes, all simulations have been completed on a multi-core, 64-bit, dual-processor machine with an NVIDIA Quadro K2000 GPU. The local configuration used in this work utilizes GCC 4.4.7 and CUDA 4.0.8 compilers.

I have focused on four different softened potential prescriptions to describe the two-body interactions that model the motions of each cluster’s center-of-mass. The first three belong to a class of prescription sometimes referred to as ‘Plummer-like’ softenings. These are the type of softening implemented in NBODY2. Prescription

one is described by

$$\begin{aligned} \mathbf{F}_1 &= -\frac{Gm_1m_2}{(r + \delta_1)^2} \hat{r}, \\ U_1 &= -\frac{Gm_1m_2}{r + \delta_1}, \end{aligned} \quad (1)$$

where r is the separation distance and \hat{r} is the direction from one mass to the other. The gravitational constant G is set to unity in this work and the masses $m_1 = m_2 = 1/2$ when referring to the masses of clusters. Prescription two is described by

$$\begin{aligned} \mathbf{F}_2 &= -\frac{Gm_1m_2}{(r^2 + \delta_2^2)} \hat{r}, \\ U_2 &= \frac{Gm_1m_2}{\delta_2} \left[\arctan\left(\frac{r}{\delta_2}\right) - \frac{\pi}{2} \right]. \end{aligned} \quad (2)$$

Note that this is not a useful potential, as it does not reduce to the Newtonian point-mass potential for $\delta_2 = 0$. However, the force expression is Newtonian in that limit, allowing particle trajectories to be integrated. The third Plummer prescription is described by

$$\begin{aligned} \mathbf{F}_3 &= -\frac{Gm_1m_2r}{(r^2 + \delta_3^2)^{3/2}} \hat{r}, \\ U_3 &= -\frac{Gm_1m_2}{(r^2 + \delta_3^2)^{1/2}}. \end{aligned} \quad (3)$$

The choice of these three prescriptions is not intended to be exhaustive but merely representative of the kinds of softenings one might adopt.

The fourth prescription is a version of the ‘spline’ softening idea discussed by Hernquist & Katz (1989) in the context of smoothed particle hydrodynamics. Based on a smoothing kernel function described in Monaghan & Lattanzio (1985), GADGET-2 smooths two-body interactions by assuming that the interacting particles are actually distributed masses “smeared” by

arXiv:1507.08518v3 [astro-ph.IM] 14 Jun 2016

the smoothing kernel. The smoothing kernel complicates the potential and force expressions far beyond those above for the Plummer prescriptions; the details of their derivation may be found in Springel *et al.* (2001). Generally, the spline softening approach uses three different approximations to the force, depending on the separation of the particles. This behavior allows spline softened forces to exactly equal Newtonian values when particles are adequately separated. With Plummer softenings, the softened force is never exactly Newtonian, even though the difference becomes computationally negligible with adequate separation. In GADGET codes, the softening length is different than the smoothing parameter, and I have adopted the same multiplicative factor to connect them. As highlighted in Springel (2005), this guarantees that the spline softened potential caused by a point mass when $r = 0$ is the same as that for a Plummer softened potential.

Much of the basic physics of cluster-cluster interactions has been investigated in-depth over the past several decades. Early analytical attempts at describing the impact of a passing mass on a spherical system (*e.g.*, Spitzer 1958; Alladin 1965) informed more numerical studies of the phenomena (*e.g.*, Roos & Norman 1979; Aguilar & White 1985, and references therein). It is not the goal of this paper to revisit or duplicate the types of studies represented by these previous works. They are important to the present work only in the sense that they provide guideposts for the behavior of the clusters in the NBODY6 simulations. As each cluster’s center-of-mass in this work is intended to represent a point mass present in collisionless N -body simulations, I focus on initial conditions that lead to hyperbolic orbits. The clusters here are intended to slide past one another without the possibility of becoming bound. I envision these clusters being what one would see if a microscope could be used to magnify the inner structure of individual masses in an N -body simulation that utilizes force softening.

Previous discussions of softening in N -body simulations can be grouped into different categories. Some researchers have focused on optimizing softening lengths to accurately reproduce forces and/or minimize computational requirements (Romeo 1998; Athanassoula *et al.* 2000; Power *et al.* 2003). Others have discussed more fundamental issues related to the appropriateness of Plummer-like softening formulas (Dyer & Ip 1993; Gerber 1996) or re-interpreting softening prescriptions as smoothing operations (Barnes 2012). The work presented here likewise investigates the impact that smoothed forces can have on the dynamics of an N -body system. My addition to this chain is the investigation of how adequately softened point-mass motions can model extended cluster center-of-mass motions. In a practical sense, the results of this work will hopefully inform the choices of future N -body simulators. For example, if comparable dynamical accuracy can be achieved with smaller computational effort, perhaps a simple Plummer softening prescription would be more attractive than the (relatively) more complicated spline prescription.

To begin, I present numerical details of the initialization procedures (§ 2.1) and the evolutions (§ 2.2). Discussions of the main analyses of the dynamical evolutions and the key results that follow form the majority of Section 3. Finally, I present a summary of the techniques

and outcomes in Section 4.

2. NUMERICAL DETAILS

2.1. Initial Conditions

Clusters are composed of N_c particles, where $N_c = 2^7$ and $10 \leq \eta \leq 14$, but $\eta = 13$ ($N_c = 8192$) has been adopted as the standard value. The positions of the particles in one cluster are randomly chosen according to a spherical density distribution with maximum radius $R_c = 1$. This work investigates clusters with equilibrium Plummer distributions (Plummer 1911) with scalelength equal to one-tenth of R_c and Gaussian distributions. The scalelength of the Gaussian distributions used is generally set to $R_c/\sqrt{5}$; this makes the Gaussian clusters less centrally concentrated than the Plummer clusters. Particles are given equal masses such that the total mass of a single cluster is $M_c = 1/2$. For Plummer clusters, thermal velocities are isotropic and speeds are chosen from the Maxwellian speed distribution. An upper limit to particle speed is given by $3v_{r,\text{rms}}$ at the appropriate radial location. With this choice, a single cluster is initially closer to virial equilibrium than if the upper limit were set to the escape speed ($2v_{r,\text{rms}}$, *e.g.*, Aarseth *et al.* 1974). Particle velocities in Gaussian clusters are chosen to be isotropic and so that the cluster is in virial equilibrium. Dynamical evolutions of isolated, single clusters show a very modest mass loss; $\Delta M_c/M_c \approx 1$ per cent for $N_c = 1024$ and $\Delta M_c/M_c \approx 0.5$ per cent for $N_c = 16384$. For single cluster NBODY6 evolutions, particles escape if they reach distances of 10 half-mass radii from the center of the cluster. The isolated cluster evolutions show evidence of some outer envelope expansion. The radius that contains 95 per cent of the mass of the cluster increases by approximately 5 per cent during an evolution lasting 10 single-cluster crossing times. For comparison, the radius containing 75 per cent of the mass increases by less than 1 per cent.

Once a single cluster has been initialized, its center-of-mass location is moved from the origin and a mirror image of the cluster is created (different particle distributions can be chosen for the two clusters; see Section 3.5). Particle velocities are simply mirrored as well. Unless otherwise noted, initial center-of-mass separations in the x -direction Δx_{init} are equal to four times the initial cluster radius R_c , while there is no offset in the y -direction. The majority of simulations I have performed have center-of-mass separations in the z -direction (impact parameters) Δz_{init} that range between one and five times R_c , but values up to $40R_c$ have been investigated.

With all particle initial locations specified, the total potential energy U_{total} is determined. The self-potential energy of a cluster is the potential energy determined between all particles in that cluster. The total potential energy is the sum of the two cluster self-potential energies and an inter-cluster potential energy determined between particles in the different clusters. The speeds of each cluster’s center-of-mass are defined as fractions of U_{total} ,

$$v_{\text{CM,initial}} = \sqrt{QU_{\text{total}}}, \quad (4)$$

where $0.2 \leq Q \leq 1.5$ for the majority of the simulations discussed here. To provide some context to the Q values, I have compared the average thermal speed of particles in a Plummer cluster to the initial relative

center-of-mass speed for clusters. The average thermal speed is that of an equilibrium Plummer sphere and is invariant to different cluster initial conditions. Varying the initial center-of-mass separation changes the inter-cluster potential energy, but by a very small amount relative to the self-potential energies. As a result, the total potential energy is roughly equal to twice the self-potential of an equilibrium Plummer sphere, and the ratio of thermal to relative center-of-mass speeds is essentially just a function of Q ,

$$\frac{v_{\text{CM,relative}}}{v_{\text{thermal}}} \approx 2.2\sqrt{Q}. \quad (5)$$

Specifically, Q values of 0.2, 0.5, 0.8, and 1.5 result in ratios of 1.0, 1.6, 2.0, and 2.7, respectively. The less-concentrated nature of the Gaussian clusters makes their potential energies smaller than those of Plummer clusters, with a corresponding reduction in the center-of-mass speeds of Gaussian versus Plummer clusters at a given Q .

The initial center-of-mass velocities are chosen to lie in the x -direction. Finally, particles in each cluster have the appropriate center-of-mass velocity added to their pre-existing, thermal velocity. With all velocities assigned, an evolution timescale is calculated from,

$$t_{\text{dyn}} = \sqrt{\frac{(2M_c)^5}{(2|E_{\text{total}}|)^3}}, \quad (6)$$

where E_{total} is the sum of U_{total} , the center-of-mass kinetic energies of the clusters, and the thermal kinetic energies of the clusters.

2.2. Simulations

The NBODY6 code advances all particles without softening their interactions. All simulations have been evolved for a minimum of ten timescales. For Gaussian and Plummer clusters with $Q = 0.2$ (lower $v_{\text{CM,relative}}$ values), simulations have been extended to twenty and fifteen timescales, respectively. Visualizations of cluster interactions show that these values provide sufficient time for clusters to reach a point of minimum center-of-mass separation and then clearly separate. With the very different initial conditions involved in the binary cluster evolutions, the escaping particle criterion has been changed from the NBODY6 default behavior. For interacting cluster simulations, particles escape only if they reach distances 50 times the quantity $(2M_c)^2/U_{\text{total}}$. This allows simulations with large center-of-mass separations (impact parameters up to $40 R_c$) to be performed without artificially removing particles. With this new escape criterion, very few particles are lost from systems.

During each evolution, particle positions and velocities are compiled every $0.1t_{\text{dyn}}$. The total number of particles in the system is reported at every output along with a list of particle identification numbers. By comparing lists of identifying particle numbers with the initial list, the cluster membership of each particle can be tracked. From this data, I calculate the centers-of-mass positions and velocities and then the thermal velocities of cluster particles. With those basics, I then calculate the thermal and center-of-mass kinetic energies of each cluster, the self-potential energies of each cluster, and the inter-cluster potential energy as functions of time. Total and

individual cluster angular momenta and average cluster radius values are also tabulated as functions of time.

The results of these simulations match those reported in earlier works dealing with similar systems and initial conditions (*e.g.*, Devadas Rao *et al.* 1987). Interactions with impact parameters $\Delta z_{\text{init}} > 2R_c$ are elastic in the sense that there is no change in either cluster's center-of-mass kinetic energy during symmetric time intervals centered on the point of closest approach. For smaller impact parameters that lead to overlap of the systems at closest approach, the center-of-mass kinetic energies decrease. The self-potential energies of clusters generically increase. This agrees with the increase of average radius of each cluster during an interaction. Small impact parameter cases increase the average radii by roughly 15 per cent around the point of closest approach, while larger impact parameters produce more modest changes, around 5 per cent. Since the clusters remain self-gravitating, their expansion is coupled with a decrease in thermal kinetic energy (Spitzer 1958). For larger impact parameter situations, the increase in self-potential has the same magnitude as the decrease in thermal kinetic energy. For smaller impact parameters, the loss in center-of-mass kinetic energy further boosts the self-potential change.

Cluster angular momentum changes are generally very small. No angular momentum component changes by more than 1 per cent of the initial magnitude of the system angular momentum during the time interval surrounding the point of closest approach. Another perspective on the size of these changes is that similarly sized changes occur when individual particles are lost from a cluster. Absent finite-particle-number variations, the clusters initially have zero angular momentum about their centers-of-mass. In the simulations with the smallest impact parameters, tidal interactions are able to torque them slightly. The small angular momenta acquired in these cases are oriented in the same direction as the initial total angular momentum.

3. ANALYSIS & RESULTS

3.1. Determining Softening Behaviors

For any given set of initial conditions, the motions of cluster centers-of-mass have been matched to the motions of point masses interacting via the softened potentials discussed in Section 1. Treating a softening length as a free parameter, the non-linear minimization routine *amoeba* (Press *et al.* 1994) is used to determine what value of δ produces the best representation of the center-of-mass motion. The figure of merit used by *amoeba* is a combination of least-squares deviations. The softened motion starts from the simulated cluster initial conditions, and an adaptive timestep Runge-Kutta scheme (implemented in the IDL routine *lsode*) integrates softened motion between the times at which simulated data (center-of-mass positions and velocities) exists. Given the M time values at which “data” values of $x(t_i)$, $y(t_i)$, and $z(t_i)$ produced by NBODY6 exist, *lsode* advances the point mass locations and velocities from t_i to t_{i+1} . The results shown and discussed here use a relative tolerance of 10^{-7} ; fourth- and fifth-order Runge-Kutta steps result in relative differences smaller than the tolerance. Tests using a tolerance down to 10^{-11} have also been per-

formed, but do not lead to any appreciable differences. Updating the time index i , the former final conditions become initial conditions and are recorded. In this way, a set of M corresponding softened “model” position and velocity values are produced. From these M pairs of values, figures of merit that quantify differences between data and model values can be formed. The main figure of merit used in this work is formed by comparing position values. For each cluster, the M differences between center-of-mass and softened point x , y , and z positions are calculated. In each direction, and for each cluster, the average of the squared difference values is used to form an rms deviation. The two cluster rms values are then averaged in each direction. Finally, the figure of merit is formed by summing the directional rms values. In this way, the figure of merit reflects the average positional deviation of the model from the data over the entire simulation. The optimal softening length δ_{opt} is that which produces the best agreement (smallest figure of merit) between the motion of the two clusters’ centers-of-mass and the softened point particles.

With a δ_{opt} value, the figure-of-merit landscape is searched near the minimum to provide uncertainty values. I have adopted a value of 10^{-3} as the relevant figure-of-merit change, as that is roughly the size of the error in the location of a cluster center-of-mass. In sum, a given δ_{opt} produces the best fit for a given model, and $\Delta\delta$ is determined by finding the two neighboring softening values that produce figures of merit that are 10^{-3} greater than the minimum value. Figure 1 shows a representative example of the information used to determine uncertainties. In general, prescriptions one, two, and three form quadratic-like figure-of-merit curves. Prescription four tends to produce the kind of one-sided valleys seen in Figure 1. This is unsurprising as the spline softening approach deals with ranges of softening values. What is mildly surprising is the fact that the prescription four δ_{opt} values always tend to be near the high-end of the uncertainty range. However, it is important to keep in mind that the difference in figure-of-merit values is extremely small between $\delta \approx 0$ and δ_{opt} . In all but the smallest impact parameter situations, one can safely assume a softening length of zero with prescription four. For contrast with Figure 1, Figure 2 focuses on the behavior of the prescription four figure-of-merit curve for a simulation where Plummer clusters have $\Delta z_{\text{init}} = R_c$. Very small softening values are clearly ruled out in these kinds of interactions.

This choice of figure of merit is straightforward but not unique. I have varied the calculation of δ_{opt} to use differences between velocities rather than positions. Resulting values of δ_{opt} fall within the uncertainties derived from the position-based calculations. All remaining discussions of δ_{opt} values and/or figure-of-merit values refer to the position-based approach.

3.2. Comparison of Softening Prescriptions

Two questions motivated this investigation. First, do particles interacting through softened potentials really behave like interacting clusters? Second, is any one prescription better than the others? I tackle the second question first in this section. However, note that this exercise is not determining an optimal form of softening potential, merely comparing several extant potentials.

For any simulation, four δ_{opt} values are determined, one for each prescription. I use the corresponding best-fit figure-of-merit values as a comparison tool. For 25 Plummer cluster simulations ($N_c = 8192$, $\Delta x_{\text{init}} = 4R_c$, $R_c \leq \Delta z_{\text{init}} \leq 5R_c$, $0.2 \leq Q \leq 5.0$), prescription 1 provides the best match 15 times, prescription 2 is best 4 times, prescription 3 is best 1 time, and prescription 4 is best 5 times. However, the differences between the values for the different prescriptions are generally very small. For example, in its 15 “wins”, the figure of merit for prescription 1 is, on average, smaller than its competitors by about 2×10^{-4} . For the other prescriptions, their margins of victory are roughly 100 times smaller. Since these differences are smaller than the error in determining the center-of-mass position, I conclude that all of the prescriptions provide comparable levels of match.

For a similar set of Gaussian cluster simulations, prescriptions 1 and 4 are evenly split; prescription 1 is best 8 times, prescription 4 is best 10 times. The softness of the Gaussian clusters make it more difficult to determine how much better each prescription is. In simulations with $Q \leq 0.5$ and $\Delta z_{\text{init}} = R_c$, the clusters experience strong tidal distortions. In the $Q = 0.2$ case, the two clusters actually merge during their encounter, making its analysis here worthless. Even though that case has been ignored here, it gives one the idea that figure-of-merit values will be generally larger than in the Plummer simulations, with correspondingly larger differences seen. In the 8 “wins” for prescription 1 (several of which are small impact parameter cases), the average figure of merit is about 0.01 smaller than that of its competitors. If the smallest impact parameter cases are removed, that value drops to about 10^{-3} . Prescription 4 tends to win in higher impact parameter situations, so its margin of victory of 10^{-5} is rather firm. While there is more hand-waving in this analysis, I again conclude that the prescriptions are basically equivalent in their ability to explain the center-of-mass motions of these clusters.

3.3. Optimal Softening Lengths

Figure 3 shows the results of determining the optimal softening length δ_{opt} using the four softening prescriptions given initially-equal-radius Plummer clusters with differing impact parameters in simulations where Q takes on the values 0.2, 0.5, 0.8, 1.5, and 5.0. A similar plot for Gaussian clusters is presented in Figure 4. Overall, the trend is for δ_{opt} values to decrease as the impact parameter increases. As discussed above, it is also typical to see non-zero lower limits to δ for smaller impact parameters.

In an attempt to filter out the impact of some other parameter values, I have created additional simulations with different initial separations and different cluster particle numbers. Simulations with initial separations in the x -direction twice the standard value produce $\delta_{\text{opt}}(b)$ curves comparable to those in Figure 3. Figure 5 shows how the $\delta_{\text{opt}}(b)$ curves differ between Plummer cluster $\Delta x_{\text{init}} = 8$ and $\Delta x_{\text{init}} = 4$ simulations with $N_c = 8192$. For clarity, only prescription one δ_{opt} values are shown. The level of agreement shown here is typical of what is seen for the other prescriptions and for results from Gaussian clusters.

The results of varying particle numbers using Plummer clusters with $Q = 0.5$ are shown in Figure 6. The panels isolate the different softening prescriptions, and

the different lines in each correspond to the various N_c values. Overall, the clusters with the lowest resolution ($N_c = 1024$) result in the largest values of δ_{opt} . For $N_c \geq 2048$, the values of δ_{opt} , uncertainties in δ_{opt} , and trends in δ_{opt} versus b are essentially the same.

3.4. Results of Non-optimal Softening

To investigate the impact of these $\delta_{\text{opt}}(b)$ relationships, imagine an N -body simulation with a specified softening length δ_{sim} . Depending on the adopted softening prescription, one would like to choose δ_{sim} so that the majority of interactions would accurately describe the center-of-mass motion of two clusters of particles.

For encounters with $\delta_{\text{sim}} \neq \delta_{\text{opt}}(b)$, the point masses will follow trajectories that do not match those of each cluster's center-of-mass with the same impact parameter. To clarify the outcome of such encounters, further imagine simulating three pairs of point masses with the same impact parameter b_0 . In simulation A, $\delta_{\text{simA}} > \delta_{\text{opt}}(b_0)$; in simulation B, $\delta_{\text{simB}} < \delta_{\text{opt}}(b_0)$, while in simulation C, $\delta_{\text{simC}} = \delta_{\text{opt}}(b_0)$. I imagine the C pair as centers-of-mass for two clusters, since they follow the same trajectories. With a larger softening length, the pair in simulation A will experience a smaller change in velocity than those in simulation C. In general, point-mass interactions with $\delta_{\text{sim}} > \delta_{\text{opt}}(b)$ result in motions that underestimate the change in velocity relative to true cluster interactions. Conversely, the pair in simulation B will experience a larger change in velocity compared to those in simulation C; interactions with $\delta_{\text{sim}} < \delta_{\text{opt}}(b)$ generically result in point-mass motions that overestimate the change in velocity relative to cluster interactions. If softened point-mass motions are intended to represent cluster center-of-mass motions, a single softening parameter is insufficient to correctly handle different impact parameters.

It is standard to break the velocity change experienced by interacting point masses into components parallel and perpendicular to the initial direction of relative motion. The parallel component is related to the dynamical friction a particle will experience while the perpendicular component relates to the relaxation time for the motion. In an N -body simulation with a single fixed softening length δ_{sim} , encounters where $\delta_{\text{sim}} > (<) \delta_{\text{opt}}(b_0)$ lead to weaker (stronger) dynamical friction and relaxation effects. Based on the ranges of δ_{opt} values presented above, very few situations will lead to an overestimation of dynamical friction/relaxation; $\delta \approx 0$ is within the uncertainties in nearly all simulations.

The question becomes, what is the likelihood for a particle in a softened N -body simulation to have an encounter with any given impact parameter? I take the N -body system to be a time-independent background volume density and investigate what a test particle moving through that system would encounter. The N -body system is spherical with radial extent \mathcal{R} . For a test particle on a radial orbit, I estimate the likelihood of an encounter by calculating the projected density of particles in the system. This projected density is a function of a distance R measured in a plane perpendicular to the velocity of the particle on a radial orbit. The R value is just the impact parameter for the test particle and a ring of system particles centered on the origin. The projected density integrated around an annulus provides the number of system particles within a range of impact

parameters. For a uniform density system, this annular density has a maximum value for $R_{\text{max}}/\mathcal{R} = 1/\sqrt{2}$. However, more realistic centrally-concentrated systems have maximum annular densities that occur much closer to the center. As a simple example, consider a cored power-law volume density with asymptotic behaviors similar to the Plummer law,

$$\rho = \frac{\rho_0}{(1 + r/r_0)^5}, \quad (7)$$

where ρ_0 is the maximum number density of system particles and r_0 is a density profile scalelength. In this situation, $R_{\text{max}}/\mathcal{R} \approx 0.05$ when $\mathcal{R} = 10r_0$. As a result, roughly 80 per cent of particles in such a system have $b/\mathcal{R} \lesssim 0.25$ and about 15 per cent have $b/\mathcal{R} \lesssim 0.05$. A Navarro-Frenk-White (Navarro *et al.* 1997, NFW) volume density produces a similar value of $R_{\text{max}}/\mathcal{R}$ but has a more slowly decaying annulus density curve. Roughly 80 per cent of particles in such a system have $b/\mathcal{R} \leq 0.55$ with about 10 per cent having $b/\mathcal{R} \lesssim 0.05$. Steepening the outer volume density profile to a Hernquist model (Hernquist 1990) shrinks $R_{\text{max}}/\mathcal{R}$ to approximately 0.03 and 80 per cent of particles have $b/\mathcal{R} \lesssim 0.35$. Roughly 10 per cent of particles have $b/\mathcal{R} \lesssim 0.03$ in this case.

For test particles on circular orbits, the approach is different. At any point along the orbit, the distribution of impact parameters encountered by the particle is given by the projected background density function in the vicinity of the orbit. For a set of orbit radii $0.01 \leq R_0 \leq \mathcal{R}$, I have integrated the projected density function over a circular region with radius b centered on the orbit. For the most centrally-located circular orbits investigated, the fraction of system particles with $b \leq R_0$ grows to 10 per cent when $R_0/\mathcal{R} \approx 0.04$ for the Plummer-like cored power-law volume density. With a Hernquist system profile the values are very similar, but for an NFW volume density this level is not reached until $R_0/\mathcal{R} \approx 0.08$. For larger orbits with values of $0.1 \leq R_0/\mathcal{R} \leq 0.3$, roughly 25 per cent of system particles have $b \leq R_0$, when the background is the Plummer-like density. This percentage increases to about 35 per cent for an NFW volume density. These sample calculations suggest that in an isotropic N -body system, with a mix of point masses on radial and circular orbits, it is not unreasonable to expect roughly 10 per cent of impact parameters to be small compared to the radius of the system.

I now draw connections between the cluster radius R_c , the size of a system in an N -body simulation \mathcal{R} , and the softening length. Taking the average density of one point mass spread over a cluster to be the same as the background system density ρ at a radius r , the cluster radius can be written as

$$R_c^3 = \frac{3}{4\pi\rho(r)}. \quad (8)$$

The minimum cluster radius is set by the maximum density. Adopting the density of Equation 7,

$$R_c = \left(\frac{3I}{N_{\text{tot}}} \right)^{1/3} r_0, \quad (9)$$

where N_{tot} is the total number of particles in the simu-

lation and

$$I = \int_0^{\mathcal{R}/r_0} \frac{u^2}{(1+u)^5} du.$$

For $5 \leq \mathcal{R}/r_0 \leq 50$, $I \approx 0.08$. This leads to

$$R_c \approx 0.1 N_{\text{tot}}^{-1/3} \mathcal{R}. \quad (10)$$

For an NFW background density, the right-hand side of Equation 10 is approximately twice as big. As I am being rather rough in this discussion, the factor of two is ignored and no distinction is made between the background density profiles.

For $10^5 \leq N_{\text{tot}} \leq 10^7$, commonly realized values, Equation 10 leads to $R_c \approx 10^{-3} \mathcal{R}$. Following the argument in Power *et al.* (2003), the N -body simulation should not have softened accelerations larger than the mean-field acceleration at the system edge. This leads to the requirement that

$$\delta_{\text{sim}} \geq \frac{\mathcal{R}}{\sqrt{N_{\text{tot}}}}. \quad (11)$$

Combining Equations 10 and 11,

$$R_c \lesssim 0.1 \delta_{\text{sim}} N_{\text{tot}}^{1/6}. \quad (12)$$

For the same range of N_{tot} mentioned above, Equation 12 leads to $\delta_{\text{sim}}/R_c \gtrsim 1$.

Combined with the previous estimates of fractions of particles encountered by test particles, approximately 10 per cent of interactions will have impact parameters less than about $40 R_c$. As this value is much larger than the range of impact parameters that have been discussed so far ($b/R_c \leq 5$), I have also run a limited number of binary cluster simulations with larger impact parameters ($b/R_c \leq 40$). The δ_{opt} values for these simulations do not show monotonic trends, but the uncertainty ranges do. The lower limits of the ranges remain near zero, but the upper limits grow roughly linearly with b .

For prescription one, the upper limits to δ stay below R_c until $b \approx 20R_c$. For prescriptions two and three, δ/R_c upper limits reach values of one at $b \approx 10R_c$. With prescription four, the upper limit to $\delta/R_c \approx 1$ when $b \approx 2R_c$. The inference I draw from these results is that adoption of the Power argument for choosing a simulation softening length will lead to underestimating violent relaxation and relaxation effects in a very small percentage of interactions, those with very small impact parameters.

One must be careful to not push this very simple analysis too far. In an actual situation with clusters interacting as parts of a much larger system further complications arise. In particular, tidal forces can affect the rates of separation of each cluster's center-of-mass (*e.g.*, Priyatikanto *et al.* 2016, Figure 1). A quick calculation suggests that the results presented here would not change dramatically in the presence of a background potential. Giving the background system a constant density (as in the core of an pseudo-isothermal halo) leads to a differential gravitational acceleration field that is constant,

$$\left. \frac{dg}{dr} \right|_{\text{background}} = \frac{GM}{\mathcal{R}^3}, \quad (13)$$

where \mathcal{M} is the mass of the background system and $G = 1$ will be assumed from here on. I note that a cuspy

distribution with a background density that is inversely proportional to radius produces no differential accelerations. Taking the background system to be composed of N other clusters, $\mathcal{M} = NM_c$. With the relationships developed earlier in this section, I estimate

$$\left. \frac{dg}{dr} \right|_{\text{background}} = \frac{M_c}{(10R_c)^3}, \quad (14)$$

where $N = 10^6$ has been adopted, in agreement with the other relationships. For comparison, I take the differential gravitational acceleration due to a neighboring cluster to be that of a point mass (since the clusters should not overlap),

$$\left. \frac{dg}{dr} \right|_{\text{cluster}} = \frac{-2M_c}{(\alpha R_c)^3}, \quad (15)$$

where αR_c is the distance from the center of the cluster. Taking a cluster to have these two contributions to tidal forces, we see that the relative strengths are comparable for $\alpha \approx 10$. As $\alpha < 10$ at the points of closest approach for the simulations presented here, I estimate that background tidal effects should be a small perturbation. With an eye toward future work, note that Priyatikanto *et al.* (2016) highlight that the details of the orientations of cluster orbits with respect to the larger system (*i.e.*, radially or tangentially biased) are important for accurate determination of tidal effects. Such an expansive investigation is far beyond the scope of the present work.

3.5. Repeated Interactions

The expansion of clusters that accompanies interactions leads to the question of how cluster size affects the softening behavior. Specifically, if earlier interactions had expanded a cluster, will a subsequent interaction with an unexpanded cluster still be modeled by the same $\delta_{\text{opt}}(b)$ relationship? I note that adopting this as a physical picture requires one to think of clusters as self-gravitating systems that remain too small to be resolved in a larger-scale simulation.

I have taken two approaches towards dealing with this situation. These simulations all start with the same center-of-mass initial conditions as the previously discussed same-radius simulations. In the first approach, one of the clusters is allowed to have an outer radius twice as big as the other. The Plummer profiles of the two clusters are defined by the same scalelength, but one can be populated out to a larger radius. These different-radius-same-scalelength simulations model situations where previous encounters have tidally extended the envelope of a cluster without affecting its core. The second approach assumes that the cluster core has also been strongly affected, with one cluster having twice the Plummer scalelength and outer radius of the other.

Differences between the three families of simulations are evident in their energy and radius-change histories. Energies in the different-radius-same-scalelength simulations behave very much like those in the previously discussed same-radius cases (see Section 2.2). In the different-radius-and-scalelength simulations, energy values are now very different between the clusters, but the self-potential energy changes are still roughly of the same magnitude as the thermal kinetic energy changes in each

cluster. Clusters in all simulations expand as a result of their interactions. As with the same-radius situations, each cluster experiences a comparable fractional increase in radius in the different-radius-same-scalelength cases. For the different-radius-different-scalelength situations, the larger cluster experiences a smaller fractional increase in size compared to the small cluster but maintains the largest size throughout the simulation. Despite these differences, the $\delta_{\text{opt}}(b)$ relationships derived from the different-radius simulations are basically identical to those from the same-radius simulations. Figure 7 shows how the $\delta_{\text{opt}}(b)$ relationships for same-radius, different-radius-same-scalelength, and different-radius-different-scalelength simulations with $N_c = 8192$ compare.

If the point masses of an N -body simulation were replaced with clusters that have initially identical radii, encounters would quickly result in a distribution of cluster sizes and scalelengths. From the simple cases investigated here, it is reasonable to assume that the different cluster sizes will not appreciably alter the conclusions based on the same-size encounters.

4. SUMMARY

I have modeled the motions of interacting binary cluster centers-of-mass with a set of softened potential prescriptions. These kinds of simulations have a substantial history in the literature, where they have been used to investigate galaxy-galaxy interactions in galaxy clusters (*e.g.*, Roos & Norman 1979; Aguilar & White 1985). The simulations discussed here are unique in that they cover a very different region of interaction parameter space and no softening is employed in the evolution of the clusters.

The main inferences drawn from these simulations are:

- Cluster centers-of-mass follow trajectories that can be well-described by point masses moving under the influence of softened potentials.
- The softening prescriptions studied here provide matches to cluster center-of-mass motions that are comparable. Differences in the qualities of the fits provided by each prescription are generally smaller than the uncertainty in a cluster center-of-mass position.
- Optimal softening lengths can be found for any cluster-cluster interaction by minimizing discrepancies between cluster centers-of-mass trajectories and softened point-mass motions. For the Plummer prescriptions, optimal softening length values are largest for the closest encounters. For the spline prescription, the optimal softening length values grow nearly linearly with impact parameter. Independent of prescription, uncertainties in the optimal values grow with the impact parameter. Softening lengths near zero fall within the uncertainties for all but the closest encounters.
- Given a prescription, the relationships between softening length and impact parameter for cluster interactions are robust against significant changes to initial conditions: cluster particle number, initial

separation distance, relative velocity, and internal structure.

- Softened point-mass interactions correctly describe cluster centers-of-mass motions when the softening length is optimal. For softenings less than the optimal value, the point masses experience more relaxation and dynamical friction effects than interacting clusters would. With softenings larger than optimal, point masses experience weaker two-body interactions than clusters would.
- A negligible fraction of the interactions experienced by point masses in an N -body simulation will have impact parameters that place them in the regime of experiencing weaker relaxation and dynamical friction effects than would clusters. However, collapse simulations that involve varying numbers of particles with given impact parameters will most likely be affected differently, possibly more severely, than the static situations discussed here.

ACKNOWLEDGEMENTS

Many thanks to UW-L student Jacob Gloe for his efforts towards optimizing the graphics-processing-unit-enabled NBODY6 code for local use and suggesting the idea for the investigation. I am indebted to an anonymous referee for numerous scientific and editorial suggestions that have strengthened this article. Thanks also to an anonymous colleague for pushing me to find an error in an earlier version of the analysis software. This work was partially supported by a University of Wisconsin — La Crosse Faculty Research award.

REFERENCES

- Aarseth, S. 2001, *New A*, 6, 277
Aarseth, S. 2003, *Gravitational N-body Simulations* (New York, NY: Cambridge Univ. Press)
Aarseth, S.J., Henon, M., and Wielen, R. 1974, *A&A*, 37, 183
Aguilar, L.A. and White, S.D.M. 1985, *ApJ*, 295, 374
Alladin, S.M. 1965, *ApJ*, 141, 768
Athanasoula, E., Fady, E., Lambert, J.C., and Bosma A. 2000, *MNRAS*, 314, 475
Barnes, J.E. 2012, *MNRAS*, 425, 1104
Devadas Rao, P., Ramamani, N., and Alladin, S.M. 1987, *Journal of Astrophysics and Astronomy*, 8, 17
Dyer, C.C. and Ip, P.S.S. 1993, *ApJ*, 409, 60
Gerber, R.A. 1996, *ApJ*, 466, 724
Hernquist, L. 1990, *ApJ*, 356, 359
Hernquist, L. and Katz, N. 1989, *ApJS*, 70, 419
Monaghan, J.J. and Lattanzio J.C. 1985, *A&A*, 149, 135
Navarro, J., Frenk, C.S., and White, S.D.M. 1997, *ApJ*, 490, 493
Nitadori, K. and Aarseth, S. 2012, *MNRAS*, 424, 545
Plummer, H.C. 1911, *MNRAS*, 71, 460
Power, C., Navarro, J.F., Jenkins, A., *et al.* 2003, *MNRAS*, 338, 14
Press, W.H., Teukolsky, S.A., Vetterling, W.T., and Flannery, B.P. 1994 *Numerical Recipes* (New York, NY: Cambridge Univ. Press)
Priyatikanto, R., Kouwenhoven, M.B.N., Arifyanto, M.I., Wulandari, H.R.T., and Siregar, S. 2016, *MNRAS*, 457, 1339
Romeo, A. 1998, *A&A*, 335, 922
Roos, N. and Norman, C.A. 1979, *A&A*, 76, 75
Spitzer, L. 1958, *ApJ*, 127, 17
Springel, V. 2005, *MNRAS*, 364, 1105
Springel, V., Yoshida, N., and White, S.D.M. 2001, *New A*, 6, 79

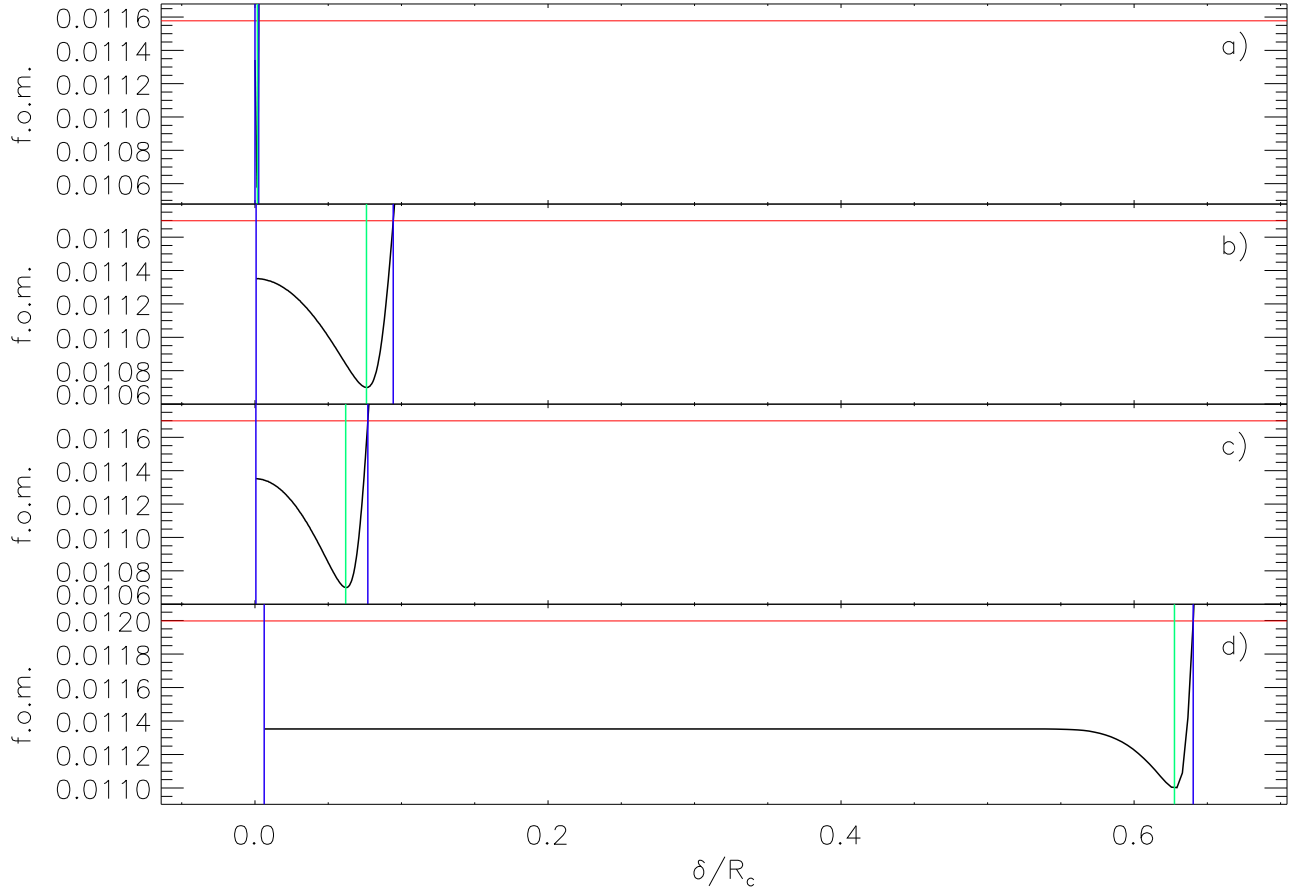


Figure 1. Panels a, b, c, and d show figure-of-merit curves for softening prescriptions one, two, three, and four, respectively. These curves are based on a Plummer cluster simulation with $N_c = 8192$, $Q = 0.2$, $\Delta x_{\text{init}} = 4R_c$, $\Delta z_{\text{init}} = 2R_c$. The thin horizontal line indicates the limiting figure-of-merit value, minimum plus 10^{-3} . The thick, solid vertical lines mark the low and high range values for the softening value, while the thick, dashed vertical line indicates the δ_{opt} value determined by the amoeba routine. Due to the rather large range imposed by the prescription 4 δ_{opt} value and the rather small δ_{opt} value for prescription 1, it is nearly impossible to see the prescription 1 curve. However, viewing that curve individually reveals it to behave very similarly to the prescription 2 and 3 curves. Note that for prescription 4 (panel d) the minimum is actually nearer the high end of the range. This is a generic behavior for prescription 4 (see, for example, Figure 3).

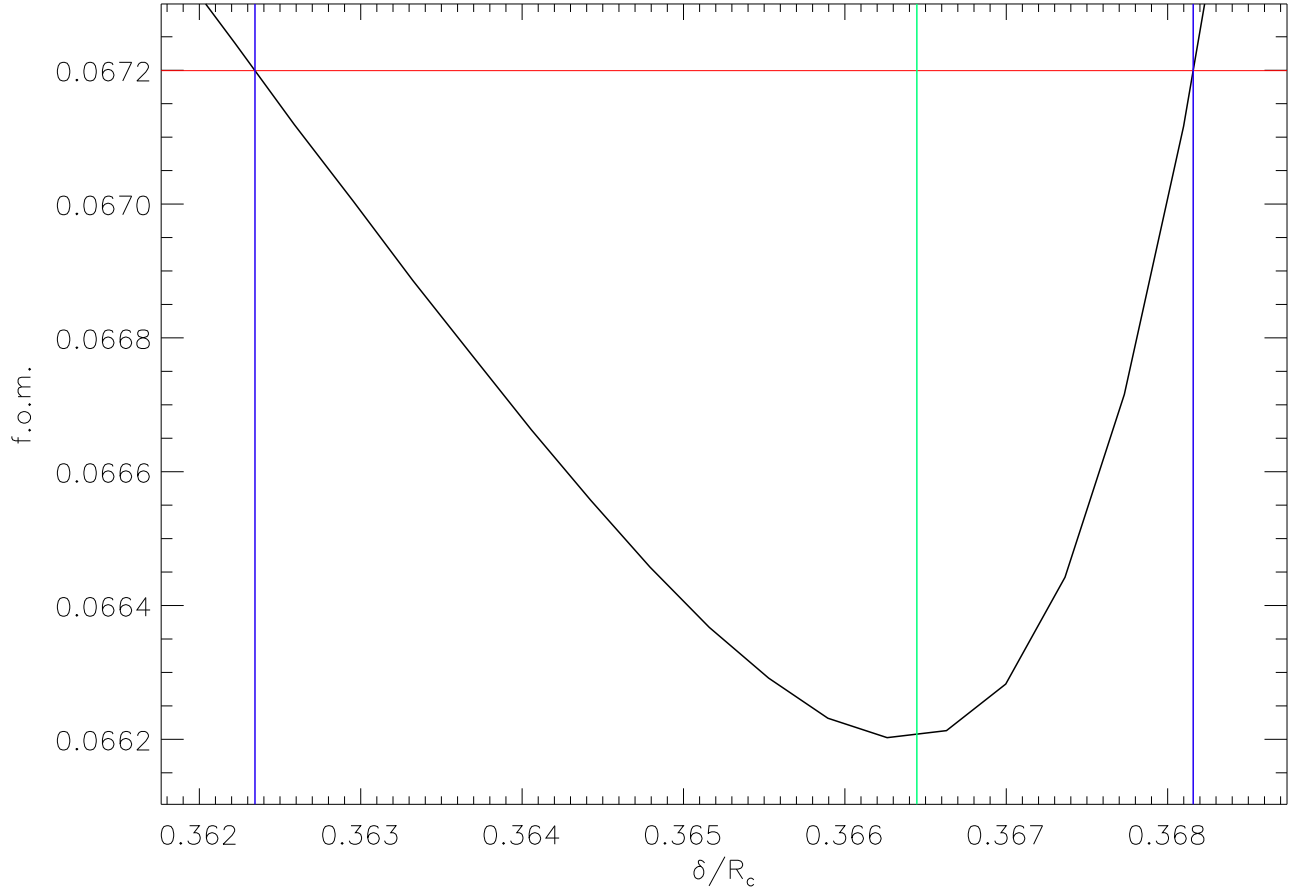


Figure 2. A single, prescription four figure-of-merit curve for a Plummer cluster interaction with $N_c = 8192$, $Q = 0.5$, $\Delta x_{\text{init}} = 4R_c$, and $\Delta z_{\text{init}} = R_c$. Contrast the quadratic-like behavior here with the one-sided trough seen in Figure 1d. Interactions with the smallest impact parameters investigated here tend to enforce lower limits to the softening length regardless of other initial conditions or cluster density profile.

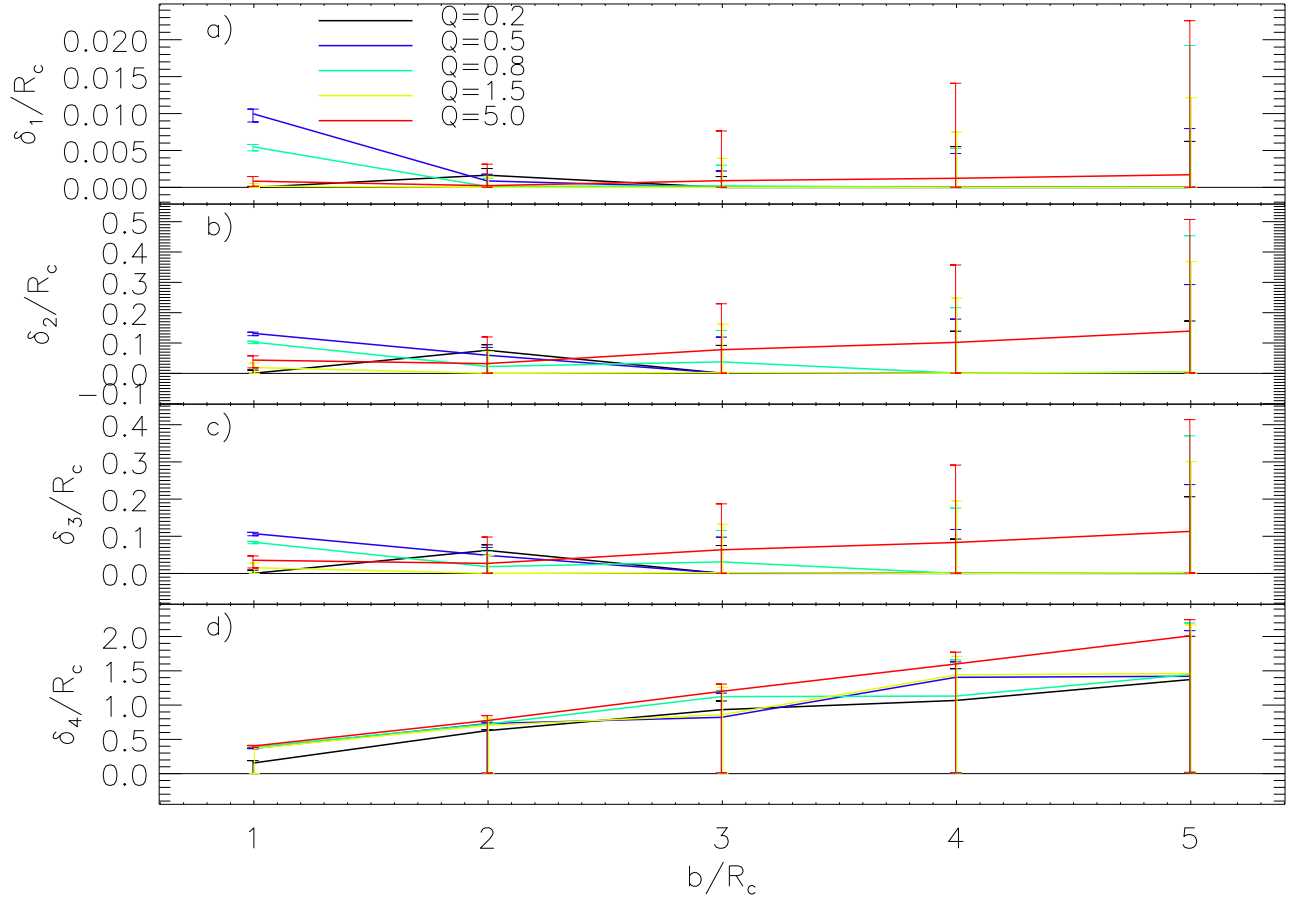


Figure 3. The relationships between the optimal softening length δ_{opt} and impact parameter for the four softening prescriptions in simulations of Plummer clusters with $N_c = 8192$. Lines connect the δ_{opt} values, while the errorbars indicate the ranges for those values. Each line represents results from simulations with different Q values. Panels a, b, c, and d correspond to prescriptions one, two, three, and four, respectively. Softening lengths and impact parameters are scaled by the initial cluster radius R_c . Uncertainty ranges grow with impact parameter. For all but the smallest impact parameter cases, softening lengths of zero are reasonable.

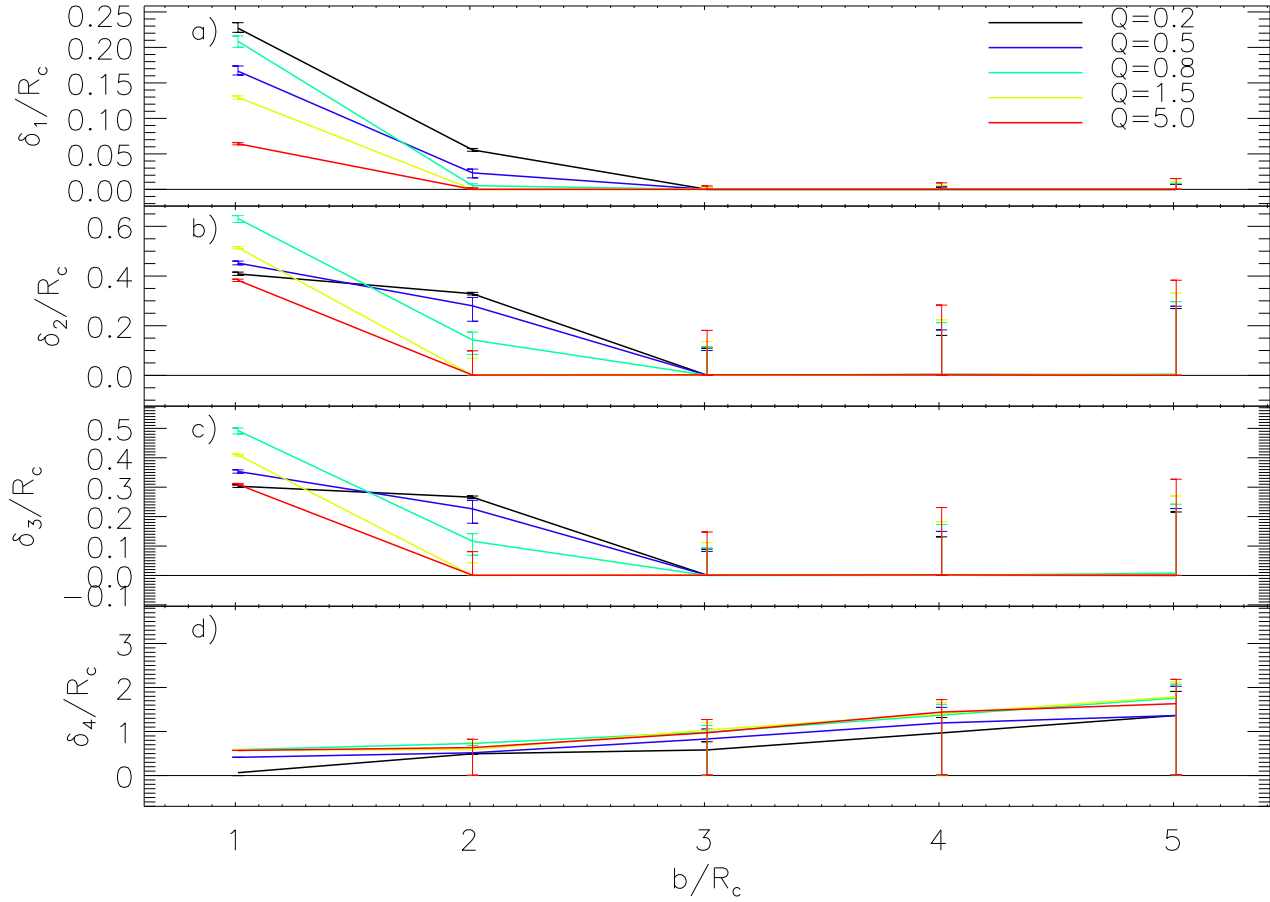


Figure 4. The relationships between the optimal softening length δ_{opt} and impact parameter for the four softening prescriptions in simulations of Gaussian clusters with $N_c = 8192$. Panels and linestyles are the same as those in Figure 3. The $Q = 0.2, b/R_c = 1$ results are not reliable as those simulations lead to cluster convergence. There is a trend for smaller impact parameter cases to result in larger δ_{opt} values. As with the Plummer clusters, softening lengths of zero are reasonable for larger impact parameter cases.

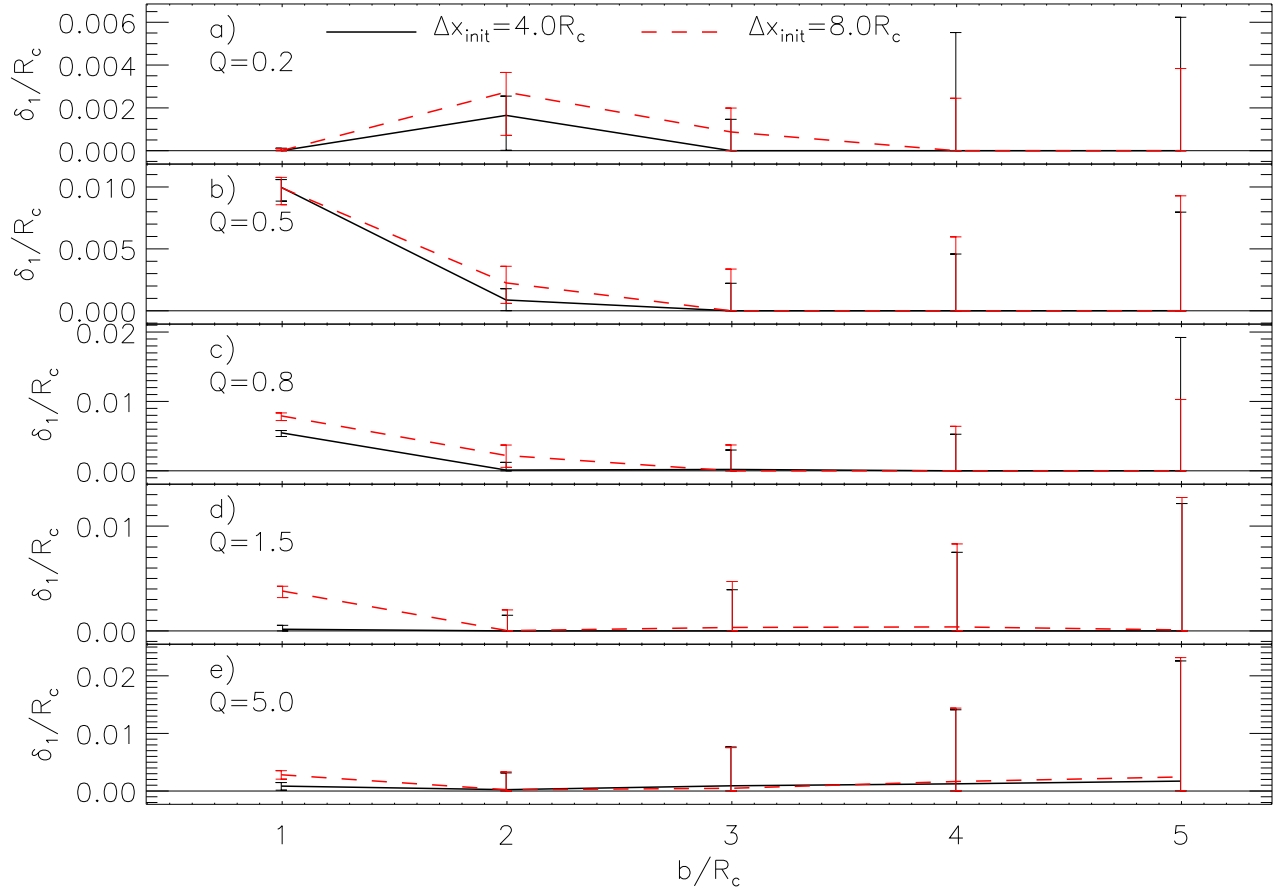


Figure 5. Comparisons between prescription one softening lengths given different initial separations in the x -direction. Panels a, b, c, d, and e correspond to results from simulations with $Q = 0.2$, $Q = 0.5$, $Q = 0.8$, $Q = 1.5$, and $Q = 5.0$, respectively. All simulations have $N_c = 8192$. Versions of this plot using information from different prescriptions and/or cluster density profile show similar levels of agreement.

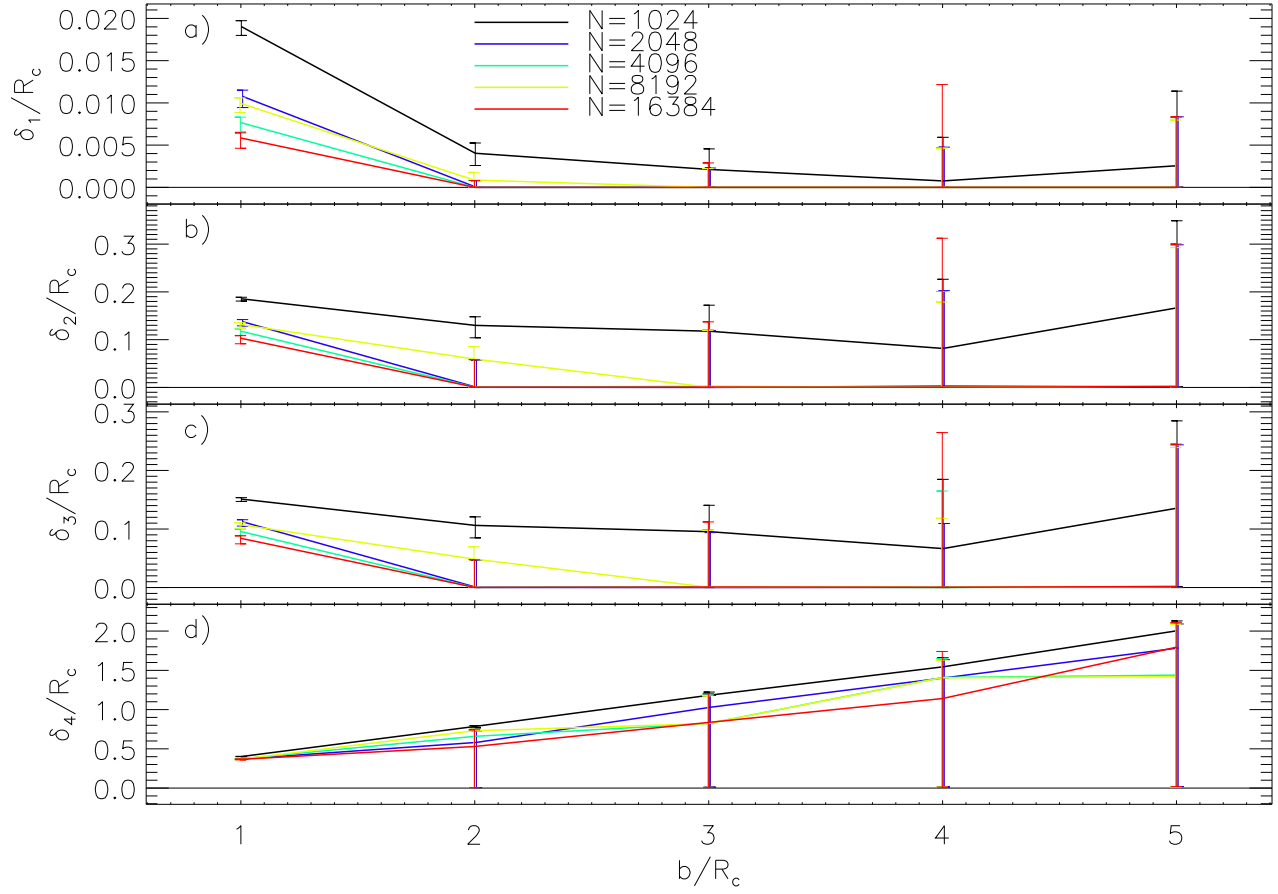


Figure 6. Comparisons between softening values given different cluster particle numbers. Panels a, b, c, and d correspond to the different softening prescriptions. The various linestyles correspond to different particle numbers $1024 \leq N_c \leq 16384$. In general, δ_{opt} values and uncertainties are consistent as long as $N_c \geq 2048$.

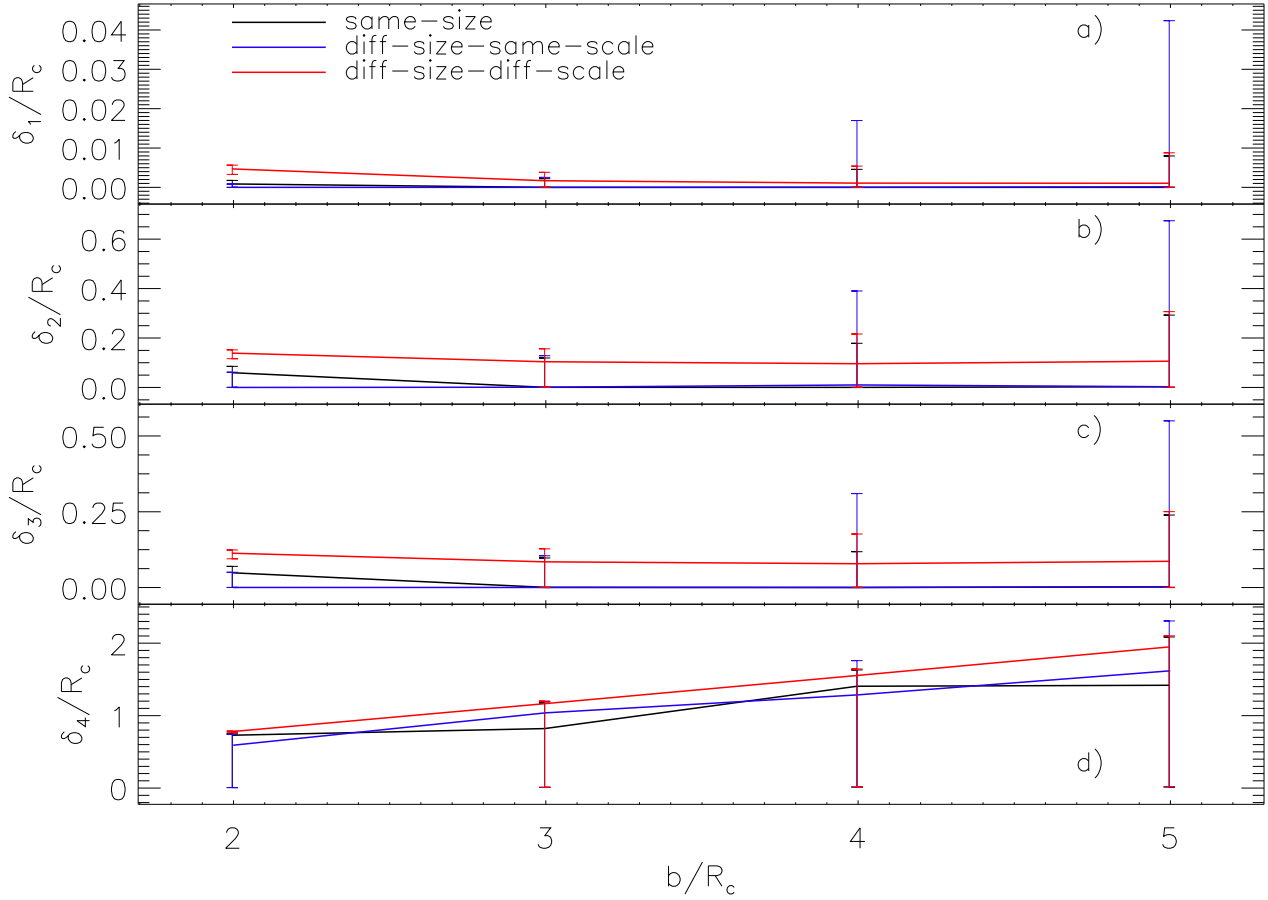


Figure 7. Comparisons between $\delta_{\text{opt}}(b)$ relationships for $N_c = 8192$, $Q = 0.5$, $\Delta x_{\text{init}} = 4R_c$ simulations in which the Plummer clusters have initially (i) same outer radii ('same-size' line), (ii) different outer radii but same density scalelengths ('diff-size-same-scale' line), and (iii) different outer radii and different Plummer density scalelengths ('diff-size-diff-scale' line). No different-size simulations have been created with $b = 1$, as they lead to excessive cluster overlap. In simulations with differences, the length in one cluster is twice that in the other cluster. For example, in the 'diff-size-same-scale' simulations, one cluster has twice the outer radius of the other. Panels a, b, c, and d correspond to prescriptions one, two, three, and four, respectively. In general, interactions with a "puffed up" cluster (larger outer radius and larger scalelength) produce larger δ_{opt} values. However, differences in δ_{opt} values are smaller than the uncertainties in all but the smallest impact parameter cases.